The Performance of a Semi-Lagrangian Transport Scheme for the Advection–Condensation Problem*

PIERRE PELLERIN,† RENÉ LAPRISE, AND ISZTAR ZAWADZKI#

Cooperative Centre for Mesoscale Meteorology and Department of Physics, University of Québec at Montréal, Montreal, Quebec, Canada

(Manuscript received 7 November 1994, in final form 8 May 1995)

ABSTRACT

A series of numerical experiments are carried out solving a coupled set of equations for advection and condensation with a semi-Lagrangian (SL) transport scheme. Canonical validation tests in one dimension show that SL suffers less numerical aberrations than many Eulerian transport schemes. Some monotonic transport constraints are experimented with. These tests confirm, for an SL transport, the statement first enunciated by Grabowski and Smolarkiewicz within the context of Eulerian transport that monotonic transport constraints are not sufficient to prevent the development of false ripples when integrating coupled field equations. A constraint is developed and successfully applied to the simplified advection–condensation problem. A two-dimensional dynamical model based on the fully elastic equations solved with a semi-implicit semi-Lagrangian scheme is used to simulate the classical moist bubble convection problem; these SL solutions are compared to published results obtained with Eulerian models.

These experiments show that 1) the original (unconstrained) SL transport scheme does produce some small ripples, 2) these ripples are smaller than with most Eulerian schemes, but 3) they may be amplified through the interaction with the condensation process when abrupt concentration changes occur; however, 4) in most applications, these ripples do not seem to contaminate unduly the results of SL simulations.

1. Introduction

With the increased availability of computers, numerical techniques can be applied to address a wide range of geophysical problems that are not amenable to direct, analytical solutions. Discretization approximations, however, cause numerical solutions to differ from truth, and a great number of studies have attempted to summarize, quantify, or reduce numerical errors—for example, Boris and Book (1973, 1976), Morse (1973), Mesinger and Arakawa (1976), and Rood (1987), to cite just a few.

Considerable attention as been paid lately to the monotonicity preservation (or lack thereof) with numerical schemes applied to the advection problem. Nonmonotone numerical schemes produce spurious ripples in the transported fields. Some of these ripples may appear as undershoots below the physically realizable value of some fields; negative concentrations, for example, can be produced locally due to the nonmonotone character of some transport schemes. Fictitious supersaturation can also result from overshoots in numerical transport schemes.

Smolarkiewicz (1983) and Smolarkiewicz and Clark (1986) exploited the naturally monotone, and hence positive-definite, nature of first-order upstream schemes to devise the Multi-directional Positive Definite Atmospheric Transport Algorithm (MPDATA): an iterative correction of higher-order errors in this scheme reduces the inherent damping associated with the upstream scheme while retaining the positive-definite character of the original scheme, at the expense of losing monotonicity. Boris and Book (1973, 1976) devised FCT (flux-corrected transport), a nonlinear correction to the flux terms in finite-difference schemes to prevent the development of false oscillations in the solutions. Recently, Smolarkiewicz and Grabowski (1989) and Grabowski and Smolarkiewicz (1990) showed that FCT constraints could be incorporated in MPDATA. The piecewise-parabolic method (PPM) is another technique that preserves monotonicity in an alternating-direction Eulerian advection scheme (Colella and Woodward 1984). Recently, Rancic (1992) extended the PPM method to the semi-Lagrangian framework in multidimensions without alternating directions.

* Dedicated to the memory of the late André Robert who contributed so much to the development of efficient numerical methods for atmospheric models.

† Current affiliation: Division de Recherche en Prévision Numérique, Atmospheric Environment Service, Dorval, Quebec, Canada.

Current affiliation: Department of Atmospheric and Oceanic Sciences, McGill University, Montreal, Quebec, Canada.

Corresponding author address: Prof. René Laprise, Department of Physics, UQAM, P.O. Box 8888, Stn "Downtown," Montréal, Québec, Canada H3C 3P8.
E-mail: laprise@phy.uqam.ca

Williamson and Rasch (1989) showed that constrained interpolations could also be used in semi-Lagrangian transport to yield a monotone algorithm. Bermejo and Staniforth (1992) showed that simple bounds could be applied on the interpolated field to greatly reduce spurious ripples and prevent negative concentrations in advection problems treated by the semi-Lagrangian method.

Grabowski and Smolarkiewicz (1990, henceforth referred to as GS90) drew attention to the important fact that spurious numerical ripples could develop even with monotone transport schemes when forcings were added to the transport problem, due to nonlinear coupling between conservation equations through the condensation forcing term. To clearly illustrate the problem, they devised a simplified set of three coupled evolution equations for thermodynamic energy, water vapor, and cloud water content in a column subject to uniform vertical motion. Their physical system allows water vapor to condense into cloud water with release of latent heat when supersaturation develops, and cloud water to evaporate into water vapor with evaporative cooling when subsaturation prevails in cloudy regions. The monotone character of the transport scheme alone was demonstrated to be insufficient to prevent spurious ripples from developing in the numerical solutions of the coupled equations. GS90 showed that FCT limiters could be applied to incorporate information about phase-change processes. GS90 also showed the merits of casting the transport problem in terms of conservative quantities. While displaying marked improvement over other schemes, their results with this approach were not entirely devoid of spurious noise at the edge of abrupt changes in the fields.

In this paper, a semi-Lagrangian (SL) transport scheme will be subjected to a series of tests similar to those of GS90. It will be shown that, even without constraints, an SL scheme suffers less severely from spurious oscillations than do most Eulerian schemes. It will also be shown that the application of bounds as suggested by Bermejo and Staniforth (1992) for the pure advection equation is insufficient to prevent the development of spurious ripples with the set of interacting equations. The general conceptual strategy proposed by GS90 consisting of exploiting the information about the physical system to establish constraints on the entire scheme will be followed to devise a relatively straightforward constraint that effectively eliminates spurious ripples in the fields of this simplified coupled system solved with an SL transport scheme.

The paper is organized as follows. Section 2 establishes the physical problem, its analytical solution, and a numerical solution obtained with an SL transport scheme with unconstrained cubic interpolation. The results obtained with the bounds proposed by Bermejo and Staniforth (1992) and a higher-order variant of it are also considered. The reasons for the residual spurious behavior are analyzed, and, through a series of physical reasoning, the foundation for a relatively simple constraint that can be applied to eliminate spurious ripples in the coupled system is established. Section 3 describes the results of a two-dimensional moist bubble convection experiment simulated by a dynamical model solving fully elastic moist equations with a semi-implicit SL scheme; these results are compared with other published results for such an experiment. The results are summarized in section 4.

2. Advection–condensation problem

The SL numerical transport algorithm has been introduced in meteorology mainly to allow for longer time steps (e.g., Robert 1981) and, hence, to reduce the computational cost associated with the integration of numerical models. It has since been recognized, however, that this scheme offers other interesting numerical properties besides its numerical stability. Because SL suffers from little numerical dispersion, it tends to produce fields that are more "coherent," that is, relatively devoid of fictitious ripples, than most common Eulerian leapfrog transport schemes. [See, for example, a comparison of various numerical transport methods presented by Ostiguy and Laprise (1990).]

To further assess the properties of the SL scheme, an experiment proposed by GS90 to diagnose some problems detected in Eulerian models will be reproduced with an SL scheme.

a. The physical problem and its semi-Lagrangian solution

The physical problem suggested by GS90 consists of a set of coupled field equations for heat and water substance in two phases, gaseous and condensed. This problem is used as a benchmark to study the performance of the SL transport scheme:

$$\frac{d\theta}{dt} = \frac{L\theta_o}{C_pT_o} C_d$$

$$\frac{dq_v}{dt} = -C_d$$

$$\frac{dq_c}{dt} = +C_d. \tag{1}$$

Here T is the temperature, θ is the potential temperature, q_v is the water vapor mixing ratio, q_c is the cloud water content (in grams of water per gram of dry air), L is the latent heat of condensation of water, and C_p is the specific heat of air at constant pressure. The subscript o beside a variable refers to its initial value. The condensation rate C_d is determined so as to convert supersaturation into cloud water when $q_v > q_{vs}$ ($C_d > 0$) and to evaporate cloud water in subsaturated air when $q_c > 0$ and $q_v < q_{vs}$ ($C_d < 0$), where q_{vs} is the saturated mixing ratio. Only the one-dimensional, vertical ver-

sion of (1) will be considered in the following. Equations (1) are the Lagrangian equivalent of the Eulerian form presented in Eq. (2) of GS90.

Given initial conditions and the velocity field, the system (1) entirely determines the subsequent evolution of the thermodynamic state variables. Figure 1 presents an example of the evolution of an initial distribution of environmental temperature with an isentropic profile at $\theta = 302.7$ K and a relative humidity of 30%, upon which is superimposed a 160-m-deep abrupt "cloud" perturbation with water content $q_c = 0.2$ g kg^{-1}, saturated mixing ratio $q_v = q_{vs}$, and potential temperature excess of $\Delta\theta = 0.1$ K. The state of the thermodynamic variables and conversion rate C_d after 150 s under a uniform vertical motion $w = 2$ m s^{-1} are displayed on Fig. 1. (This corresponds closely to Fig. 2 of GS90.)

Equation (1) is now solved numerically by a process-splitting (fractional time step) method. In a first step, an adiabatic transport is calculated with a three-time-level semi-Lagrangian transport scheme,

$$\frac{d\psi}{dt} \approx \frac{\psi^*(z, t + \Delta t) - \psi(z - 2\alpha, t - \Delta t)}{2\Delta t} = 0, \tag{2a}$$

where $\psi \in \{\theta, q_v, q_c\}$. The vertical displacements in one time step α are computed as follows:

$$\alpha_{(z,t)} = \frac{1}{2}\int_{z-2\alpha, t-\Delta t}^{z,t+\Delta t} dz' = \frac{1}{2}\int_{t-\Delta t}^{t+\Delta t} w_{(z,t')}dt' \approx \Delta t w_{(z-\alpha,t)}. \tag{2b}$$

While (2b) must be solved iteratively for general profiles of advecting velocities, the trajectories in (2b) are trivial to evaluate with constant vertical velocities w. The values of the fields at their upstream positions

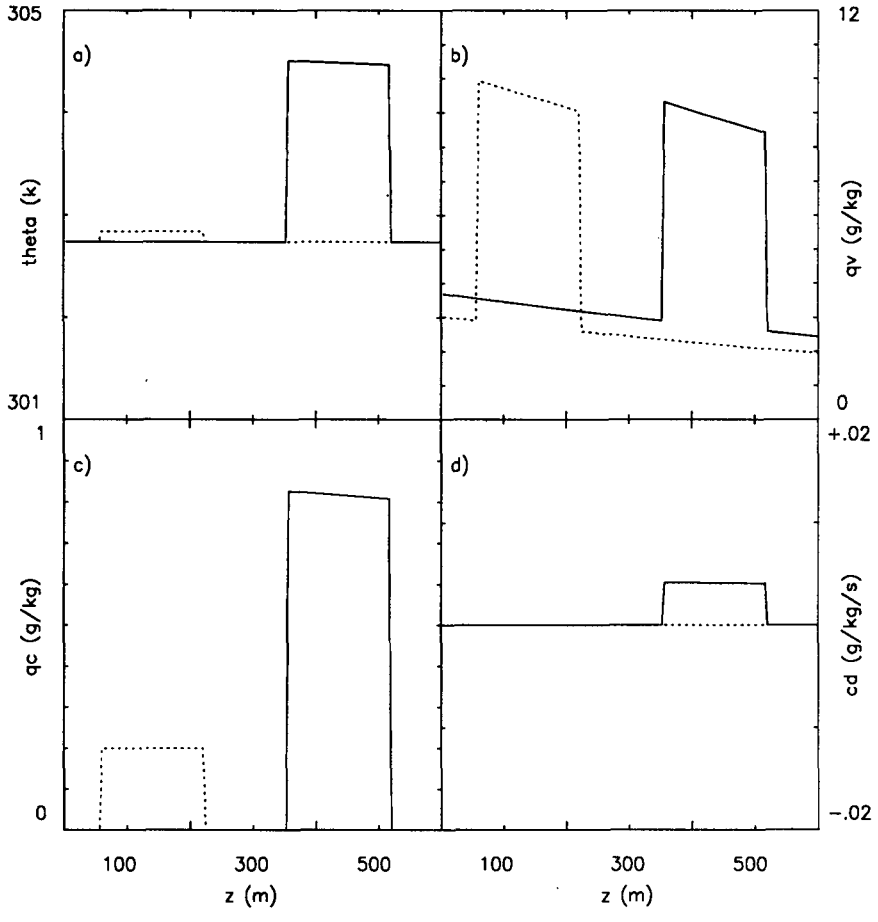

FIG. 1. Evolution of (a) vertical profiles of potential temperature θ (K), (b) mixing ratio q_v, (c) cloud water content q_c (g kg^{-1}), and (d) the associated conversion rate C_d (g kg^{-1} s^{-1}, positive for condensation of water vapor into cloud water) under a uniform vertical motion of 2 m s^{-1}. Dotted lines correspond to the initial profiles, as defined in the text, and solid lines correspond to the profiles after 150 s, according to Eq. (1).

$\psi_{(z-2\alpha,t-\Delta t)}$ are determined at each time step through a cubic interpolation of their values at the four closest grid points. Then, in a second step, the interim forecast fields ψ^* are affected by the condensation process C_ψ as follows:

$$\psi_{(z,t+\Delta t)} = \psi^*_{(z,t+\Delta t)} + 2\Delta t C_\psi[\psi^*_{(z,t+\Delta t)}] \quad (2c)$$

via a "forward" correction step. (Note that other methods are possible that would take into account the fact that the condensation process is occurring during the displacement.)

The numerical solution of (1) is performed using (2) on a mesh of $\Delta z = 4$ m and a time step of $\Delta t = 2.586$ s (for a Courant number of 1.3) for 58 time steps, corresponding to an integration of 150 s. The numerical solution thus produced is shown in Fig. 2. While the numerical solution captures the essential features of the analytical solution, it can be noted that spurious noise develops in all the fields exhibiting sharp gradient zones as a result of the approximations made in the interpolation of upstream values. It should be noted that, with discontinuous fields, increasing the order of the interpolation or reducing the mesh size is not a solution. With finer mesh (results not shown), the oscillations simply appear at smaller scale, but their amplitude is not reduced appreciably. This is analogous to the Gibbs phenomenon of Fourier series. In fact, the noise can be increased with finer mesh because more time steps are needed to perform a given length of integration if the Courant number is maintained. Overall though, the SL scheme with cubic interpolation performs better than most nonmonotone finite-difference schemes. In fact, Fig. 2 fares well even when compared to, say, Figs. 3 and 4 of GS90 obtained with oscillatory and nonoscillatory versions of the MPDATA scheme, respectively. Most of the advantage of the SL scheme derives from the small numerical dispersion associated with the interpolative nature of the scheme. The stable nature of the scheme also allows the use of longer time steps, so a given integration can be achieved in fewer steps than with Eulerian schemes.

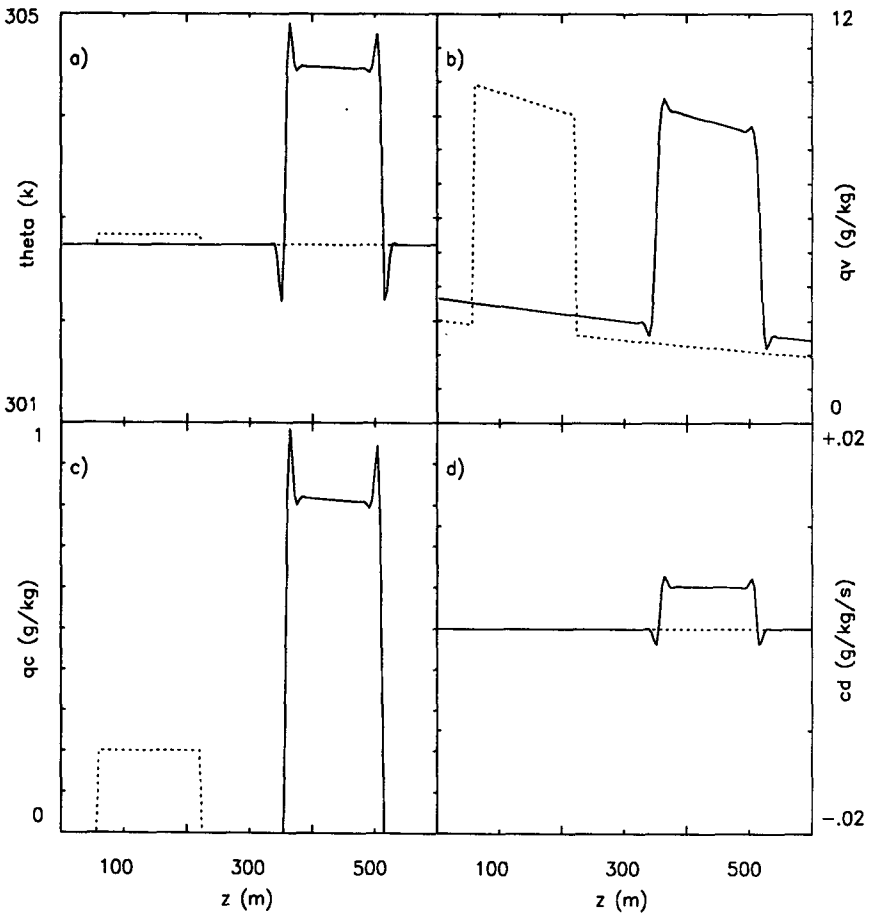

FIG. 2. As in Fig. 1 but for the numerical solution obtained with an unconstrained semi-Lagrangian transport scheme using a vertical resolution of $\Delta z = 4$ m and a time step of $\Delta t = 2.586$ s after 150 s (solid lines); dotted lines correspond to the initial profiles.

b. A bounded semi-Lagrangian transport

To confirm that the false ripples are due in part to the advection part of the coupled advection–condensation system (1), the condensation–evaporation conversion term C_d will be temporarily deactivated. Figures 3a and 3b present the results thus obtained for potential temperature and water vapor, respectively. (Note that the potential temperature excess in cloud has been increased to $\Delta\theta = 1.8$ K for this test.) By comparing Figs. 3a,b with Figs. 2a,b, it can be seen that the magnitude of the ripples in the mixing ratio field are just as important, although the ripples in potential temperature are reduced with C_d set to zero, indicating that some spurious effects in Fig. 2 also result from the nonlinear coupling of conservation equations through the conversion term.

Bermejo and Staniforth (1992) proposed a solution to control the spurious oscillations associated with the interpolation of rapidly varying fields in a pure advection test. Their solution consists of imposing bounds to interpolated fields so that an interpolated value is bounded within the range of values of the field at the grid points surrounding the interval of interpolation: whenever an interpolated value lies outside the range of values of the surrounding grid points, that interpolated value is brought back to the minimum or maximum value of these grid points, as appropriate. Figures 3c,d present the results obtained with this bounding constraint and again deactivated phase conversion. It can be seen that the application of bounds is indeed effective in preventing spurious ripples from developing in the potential temperature and cloud water distributions in this pure advection test. However, it can also be seen that the mixing ratio distribution still does suffer some subtle deficiencies in the derivative of the distribution near the edges of the discontinuity.

A close look at the mixing ratio field near the edges of the cloudy region reveals that these deficiencies are the result of the particular bounds suggested by Bermejo and Staniforth (BS). Their bounds work well when a discontinuity is flanked by constant distribution. On distributions that exhibit definite slopes near discontinuities, as is the case for the mixing ratio field that decreases with height within the cloudy region, BS bounds produce breaks in the slope of the distribution. In the following test, the BS bounds were replaced by another constraint: whenever an interpolated value lies outside the range of values of the two immediate surrounding grid points, that interpolated value is replaced by a linear interpolation between these gridpoint values. Clearly, such a linearly interpolated value will satisfy the bounding condition, since linear interpolation is monotone. The proposed linear constraint is in the FCT spirit of mixing high- and low-order schemes to achieve monotonicity. The linear constraint can be viewed as a locally first-order scheme, and BS bound as a locally zero-order scheme. Figures 3e, f show the results obtained with the proposed linear constraint (LCSL) applied to the uncoupled system of field equations. Quite clearly, the linear constraint has removed the residual deficiencies identified with the BS constraint in Figs. 3c,d.

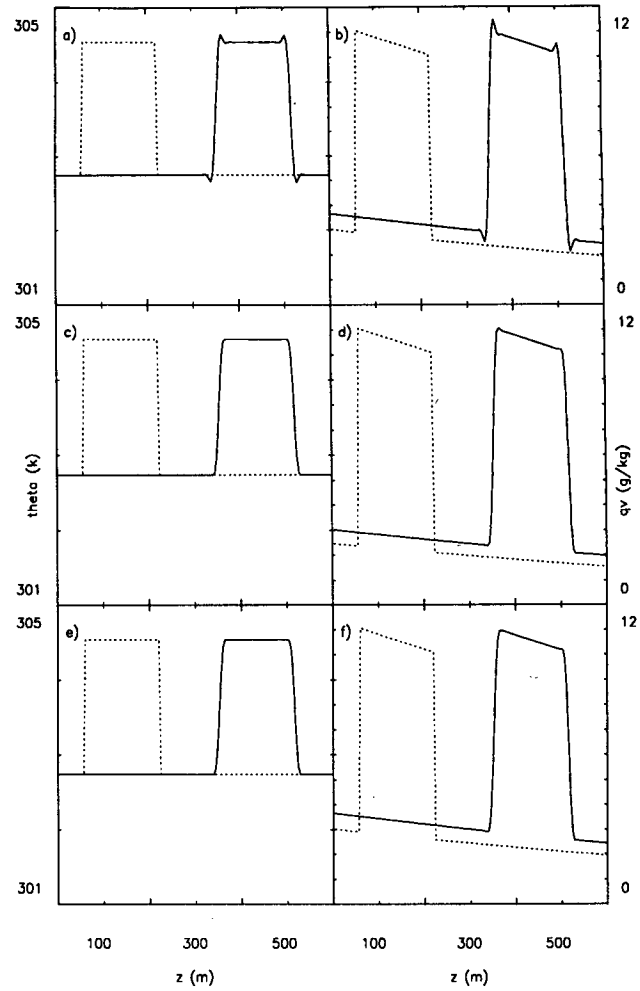

FIG. 3. (a) and (b) Numerical solution of Eq. (1) without conversion ($C_d = 0$) for potential temperature (a) and water vapor (b) obtained with unconstrained semi-Lagrangian transport scheme. (c) and (d) As above but with zeroth-order bounds applied to the advected quantities as suggested by Bermejo and Staniforth (1992). (e) and (f) As above but with first-order bounds applied to the advected quantities (LCSL). Dotted lines correspond to the initial profiles used for this test.

c. A bounded semi-Lagrangian coupled system

Satisfied of the performance of the LCSL on the pure advection problem as analyzed in section 2b, the phase conversion term is now reintroduced, and the performance of the scheme for the coupled advection–condensation system is assessed in sections 2b(1) and 2b(2).

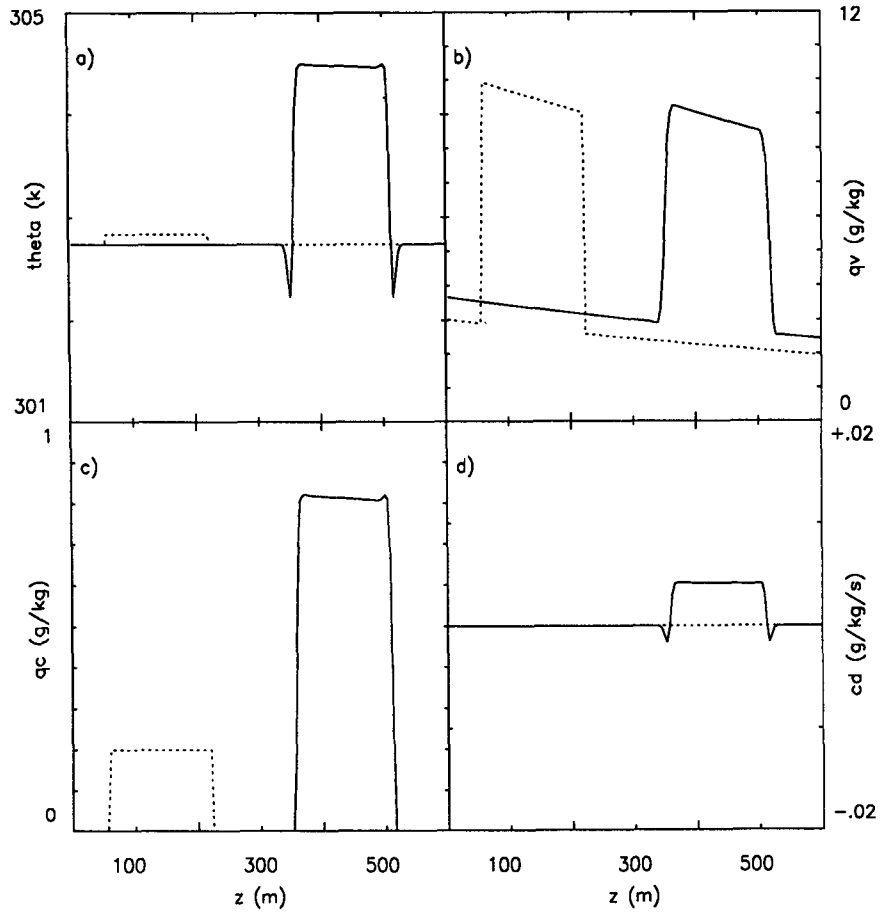

FIG. 4. Numerical solution of the coupled system [Eq. (1)] as in Fig. 2 but with linear constraint applied to the advected quantities (LCSL).

1) LINEARLY CONSTRAINED SL SOLUTION

Figure 4 presents the solution of the coupled equations obtained with the same LCSL scheme previously used for the pure advection problem displayed in Figs. 3e, f . The solutions obtained with the LCSL are clearly superior to those obtained with the unconstrained scheme displayed in Fig. 2. By including source–sink terms in the equations, however, the numerical solutions have lost their monotone character. In particular, there is fictitious cloud water evaporation and cooling at the cloud edges. The potential temperature field (Fig. 4a) is most strongly affected by this spurious effect. The loss of monotone behavior of the LCSL scheme is in conceptual agreement with the results of Grabowski and Smolarkiewicz (1990), who showed that the monotone character of a numerical scheme on a pure advection problem is not a sufficient condition for a monotone solution to a problem with sources and sinks.

2) PHYSICALLY CONSTRAINED SL

A detailed analysis of the development of ripples in the solution of LCSL for the coupled problem revealed their origin and suggested a possible ad hoc correction. At the edge of a cloud, the upstream interpolation of cloud water is performed between a "clear air" grid point with $q_c = 0$ and $q_v < q_{vs}$ and a "cloudy" grid point with $q_c > 0$ and $q_v = q_{vs}$ (q_{vs} being a function of the local temperature in each case). Quite clearly, any monotone interpolation performed separately on q_c and q_v in the transition zone will almost always result in an interpolate with values $q_c > 0$ and $q_v < q_{vs}$ locally, thus producing spurious local evaporation of cloud water and evaporative cooling at the cloud edge during the condensation–evaporation part of the time step.

The above analysis suggests a "physical" constraint that could be applied to remedy the remaining problems identified with LCSL in Fig. 4. Following the linear-bound cubic interpolation of all the constituents, the interpolated value of cloud water can be further corrected as follows. Whenever 1) cloud water is present following such an interpolation, but 2) adjacent grid points do not both have clouds, and 3) the corresponding interpolated value of mixing ratio is subsaturated at the corresponding interpolated temperature, the in-

terpolated cloud water is considered to be fictitious and accordingly it is eradicated, thus effectively preventing false evaporation from occurring there at the next condensation–evaporation time step. Mathematically, this physical, or nonlinear, constraint (NLSL) can be stated as follows:

$$\text{if} \quad \{[q_c^* > 0] \text{ and } [q_v^* < q_{vs}(T^*)] \text{ and } [q_c^a = 0 \text{ or } q_c^b = 0]\}, \quad \text{then} \quad q_c = 0, \quad (3)$$

where the superscript asterisk, a, b refer to the interpolated value and to the values at adjacent grid points (above and below), respectively. The cloud water mass thus removed can either be redistributed in some ad hoc fashion or simply ignored. (Semi-Lagrangian advection is not formally conservative anyway.)

Figure 5 presents the results obtained with the NLSL scheme, using the additional nonlinear constraint (3). This result may be compared with the LCSL result previously presented in Fig. 4. It can be seen that the numerical solution of the coupled system obtained with the NLSL scheme exhibits the desired character of monotonicity, with little additional damping in the solution due to the additional constraint. This solution is in fact better than the best solution of GS90 with the nonoscillatory version of MPDATA constrained with some limiters for total water substance in cloud (GS90's Fig. 8). In fact, the solution of NLSL approaches closely the analytical solution displayed in Fig. 1 except for rounded cloud edges.

d. Further experiments with LCSL

When the results of unconstrained SL are compared to corresponding Eulerian solutions, it is noteworthy that the SL solutions exhibit far less false ripples than corresponding Eulerian schemes. This implies that these numerical ripples can most easily be eradicated by constraining the SL rather than Eulerian methods, in general. It has been shown in the first part of this section that it is possible to develop some linear and nonlinear constraints to reduce greatly the false pertur-

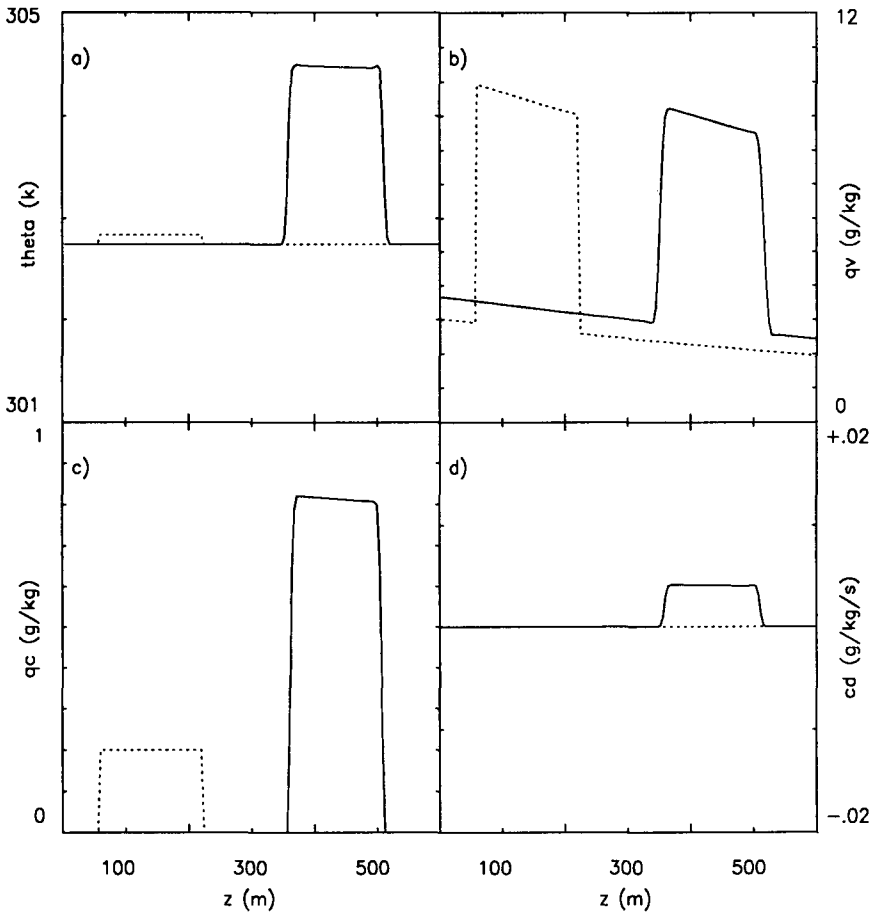

FIG. 5. Numerical solution of the coupled system [Eq. (1)] obtained with the nonlinear physical constraint [Eq. (3)] applied on a semi-Lagrangian transport scheme (NLSL). The experimental parameters are otherwise as in Figs. 2 and 4.

bations that arise in the coupled condensation–evaporation problem. It is not as easy to work with these constraints, however, and some of them may in fact create other problems in more complex systems. For example, constraint (3) would prevent the cloud mixing that physically could be taking place at the cloud edges. Ideally, one would prefer to eliminate these arbitrary constraints as much as possible.

The weaknesses of the semi-Lagrangian were identified above as being related to the geometry of the distributions of the fields, that is, the difficulty for cubic interpolation to resolve very steep gradients. One may ask the question whether the above canonical tests are at all representative of "real" cases. (How often are perfectly discontinuous distributions observed in nature?) To clarify this point, another test is made in which the discontinuity of initial distributions is spread over three grid points, analogous to the initial conditions used by Grabowski and Clark (1991). Figure 6 presents the results obtained with LCSL, that is, without the physical constraint (3). The false perturbations are almost nonexistent in the case with rounded edges. These results may be compared to those obtained with the same LCSL scheme but with the discontinuous initial distributions presented in Fig. 4. We would like to argue that simple linear constraints applied in the semi-Lagrangian scheme, such as LCSL, are sufficient to prevent the occurrence of most fictitious ripples when the distribution of the fields are "reasonable," that is, when the fields are not discontinuous. We can speculate that the situation would be more difficult with transport algorithms that have strong inherent false dispersion properties, such as most Eulerian methods; in that case, false dispersion would develop sharp gradients even if these were not initially present. Numerical dispersion can be reduced in any model by increasing the resolution. The convergence toward the analytical solution may be desperately slow though, and this option degrades the computational efficiency of the scheme.

To reinforce the point that the coupled problem is very sensitive to the initial conditions, another experiment is carried out with the same (discontinuous) ini-

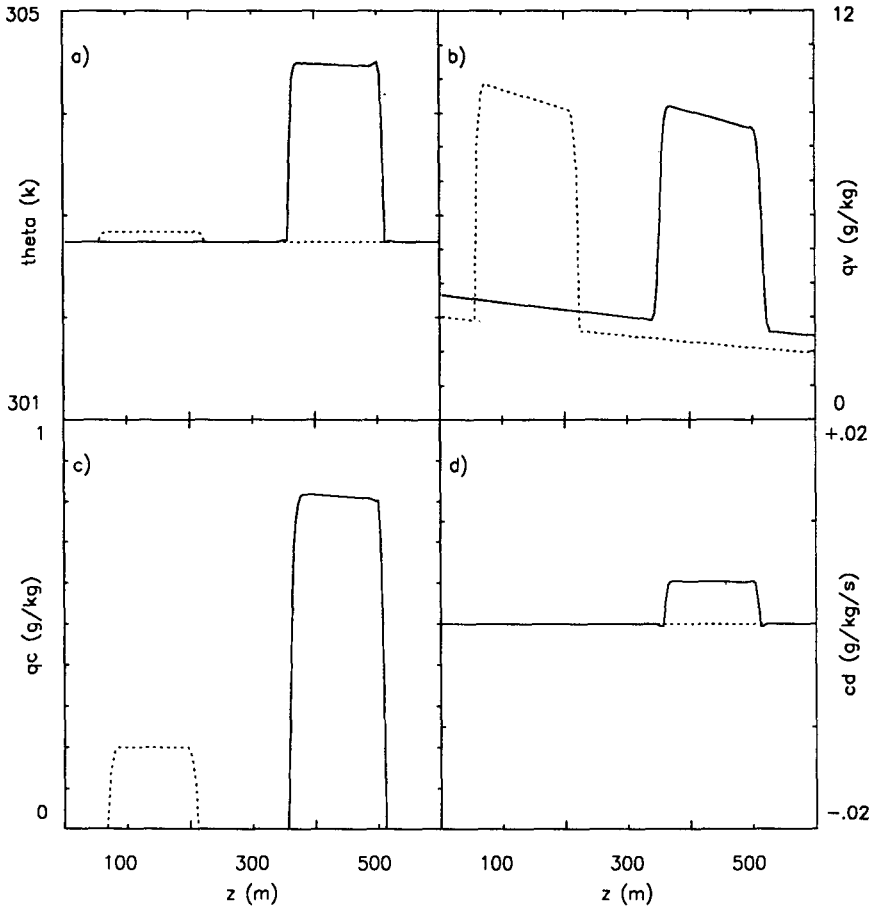

FIG. 6. Numerical solution of the coupled system [Eq. (1)] obtained with the linear constraint applied to the advected quantities (LCSL). Initial conditions differ from those used in Fig. 4 in that the sharp discontinuities in the distributions have been smoothed slightly.

tial conditions that were used to produce the results presented in Fig. 4, but this time, the initial cloud water content (a variable that is, in any event, not routinely analyzed) was set to zero. Figure 7 presents the results thus obtained with the LCSL scheme. It can be seen that the false perturbations are almost nonexistent in this simulation. The reason for this behavior is that the cloud water content that develops during the course of the integration adopts the "rounded" shape of the other thermodynamic variables as they are transported (interpolated, smoothed), and hence, no false evaporation occurs due to unrealistically sharp gradients of cloud water amount.

3. Moist convection experiment

Canonical tests are convenient to diagnose the properties of numerical algorithms; the validity of such tests, however, is limited to the narrow range of conditions under which these tests are carried out. Hence, there is a need to carry out realistic, detailed nonlinear tests to validate the hypotheses that are developed based on canonical tests. In this section, a moist bubble convection experiment will be performed with a dynamical model solving the fully elastic equations with a semi-implicit (SI) SL scheme.

The atmospheric model used for this study, SISLAM, is based on the fully elastic equations solved by an SI-SL scheme (Tanguay et al. 1990; Robert 1993). The numerical formulation of the dry part of this model is almost the same as that of the MC2 (Mesoscale Compressible Community) model developed for CCRM (Cooperative Centre for Mesoscale Meteorology) (Bergeron et al. 1994). This SI-SL numerical strategy has been shown to allow a high computational efficiency without having to approximate the field equations to filter the fast-moving elastic modes. The two-dimensional version of this model is used here in its moist version, solving (1) interactively with the dynamical momentum equations. Subgrid-scale mixing will be represented using a prescribed constant eddy-mixing coefficient K, as in Grabowski and Clark

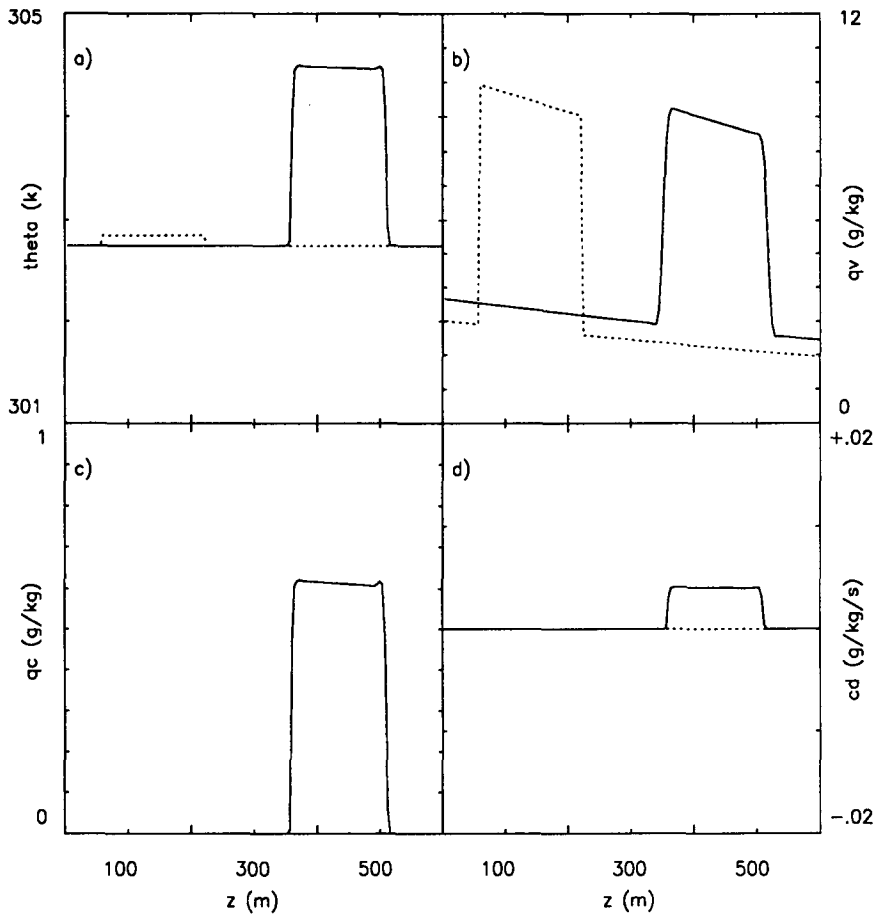

FIG. 7. Numerical solution of the coupled system [Eq. (1)] obtained with unconstrained SL. Initial conditions differ from those used in Fig. 2 in that the cloud water amount has been set to zero initially.

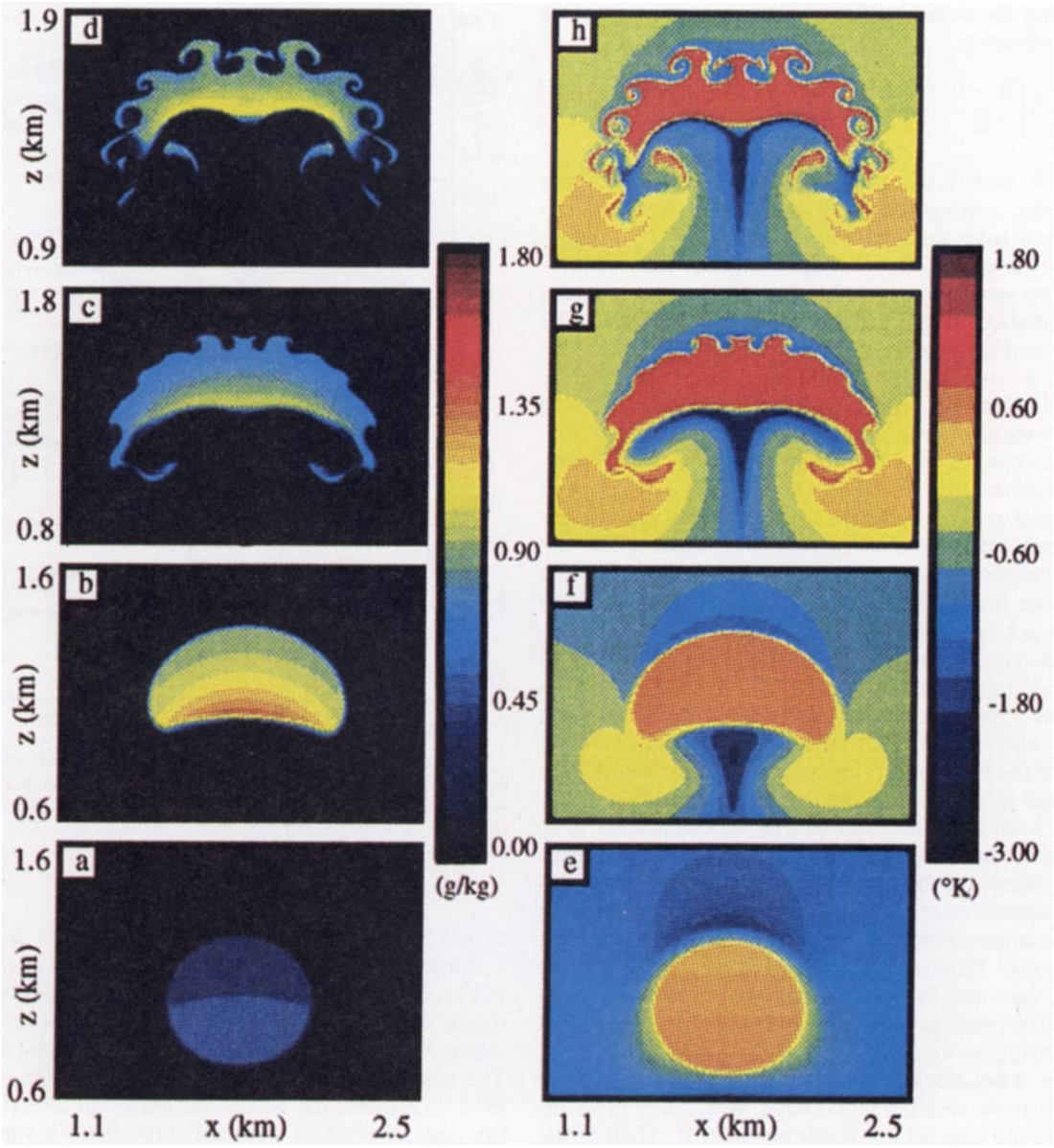

FIG. 8. Cloud water amount (left column) and buoyancy (right column) fields simulated by SISLAM with $K = 0$ and unconstrained interpolation. The fields are displayed at 2, 4, 6, and 8 min from the beginning of the integration initialized with a round saturated bubble of 600-m diameter. The resolution of the model is $\Delta x = \Delta z = 5$ m, $\Delta t = 2.5$ s. Only part of the 3.6 km × 4.8 km computational domain is displayed, centered on the rising moist bubble.

(1991). No constraints at all will be applied for these experiments.

For these tests, we attempted to reproduce the same initial conditions used by Grabowski and Clark (1991). A spherical bubble of moist air is inserted into a stable environment with uniform static stability $\partial \ln\theta/\partial z = 1.3 \times 10^{-5}$ m^{-1}, uniform 20% relative humidity, surface temperature of 283 K, and surface pressure of 850 hPa. The domain is a two-dimensional box of 3.6 km × 4.8 km delimited by free-slip solid walls. The bubble is defined as a region with higher relative humidity (RH). The RH increases smoothly from 20% to 100% in a radius varying from 200 to 300 m. The bubble is centered at 800 m above the surface initially. These simulations were performed on a computational grid with 720 × 960 grid points, with a resolution of $\Delta x = \Delta z = 5$ m and a time step of $\Delta t = 2.5$ s.

Figure 8 presents the results of a SISLAM simulation made with no explicit eddy diffusion ($K = 0$). The left and right panels present the cloud water content (g kg^{-1}) and the buoyancy (K), respectively, over a subregion of the computational domain sur-

rounding the moist bubble in its ascent. Buoyancy is here defined as

$$\bar{\theta}\left\{\frac{\theta-\bar{\theta}}{\bar{\theta}}+\left(\frac{R_v}{R_d}-1\right)(q_v-\bar{q}_v)-q_c\right\},$$

where R_v and R_d are the water vapor and dry air gas constants, respectively, and the overbar refers to unperturbed environmental values. Because of its higher relative humidity, the bubble is lighter than its surrounding environment and, hence, begins to rise and cool adiabatically, thus inducing condensation. The panels in Fig. 8 correspond (from the bottom up) to 2-, 4-, 6-, and 8-min integration times. After 2 min, condensation has begun, and the latent heat released has enhanced the initial buoyancy (orange color). The rising motion of the bubble is clearly seen after 4 min. Environmental air above the bubble has by then been lifted and cooled adiabatically, hence decreasing the buoyancy just above the bubble (blue color). The top of the bubble may be considered as a interface between light and heavy fluids. The environmental air flows downward, while the bubble continues to rise, thus creating a narrow shear zone on the sides of the (still rounded) rising bubble. After 6 min a transition occurs with the appearance of turrets on the upper part of the bubble and Kelvin–Helmoltz (K–H)-like rolls on the sides of the bubble. As time progresses, these rolls amplify and migrate down the sides of the bubble.

We would like to reiterate that no constraints were applied to the SL scheme for these moist bubble tests. It was shown in the previous section that false ripples could appear near cloud edges with SL transport but that these perturbations tend here to be less severe than with most Eulerian models. Grabowski and Clark (1991, hereafter GC91) showed that the use of coarse resolution could give rise to larger numerical noise that would trigger cloud-edge instabilities in some Eulerian models. It has also been shown by GC91 that these false perturbations near the cloud edge, when they grow intense, could prevent the development of K–H-like rolls at the proper scale. Numerical noise tends to spread tight gradient zones, and as K–H-like rolls tend to develop on spatial scales commensurate with the thickness of the shear and stability gradient zones, the scale of these rolls will be too large when the solution is contaminated by numerical noise. It is well established that numerical noise is strongly affected by eddy diffusion. GC91 showed that eddy diffusion could quench spurious rolls that would otherwise develop in simulations made with coarse resolution. The drawback is that this explicit eddy diffusion could, at the same time, prevent the development of physical rolls.

The effect of explicit eddy diffusion on the bubble simulated by the SISLAM model will now be analyzed. Figure 9 summarizes the results obtained with four eddy-mixing coefficients, K = 0, 0.25, 0.5 and 1.0 m^2 s^{-1}, and for two spatial resolutions, $\Delta x = \Delta z$ = 10 m and 5 m. (The simulation with K = 0 and $\Delta x = \Delta z$ = 5 m corresponds to the solution previously presented in Fig. 8.) Our SL results suggest, as in GC91, that the use of coarse resolution gives rise to larger numerical noise, which in turn excites cloud-edge instabilities. The use of the large eddy-diffusion coefficient (K = 1 m^2 s^{-1}) reduces the numerical noise but also prevents the development of physical rolls. With a somewhat smaller coefficient (K = 0.5 m^2 s^{-1}), some eddies (probably a mixture of numerical and physical eddies) begin to appear at the cloud edge. When the diffusion coefficient is further reduced (K = 0.25 m^2 s^{-1}), the cloud-edge eddies then become clearly visible. These are of larger dimension in the coarse-resolution experiment. Without explicit diffusion, turrets and rolls develop at both resolutions. They are again of larger dimension in the coarse-resolution experiment.

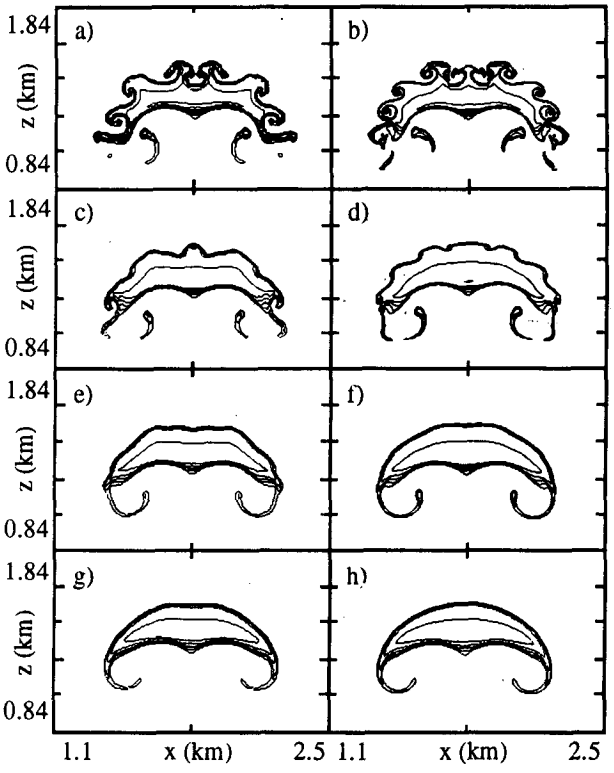

FIG. 9. SISLAM simulated cloud water amounts after 7 min at two resolutions (left column: $\Delta x = \Delta z$ = 10 m; right column: $\Delta x = \Delta z$ = 5 m) and with four different eddy-mixing diffusion coefficients (first row, K = 0; second row, K = 0.25; third row, K = 0.5; last row, K = 1.0 m^2 s^{-1}).

These SL results may be compared with those of GC91 obtained for similar conditions with a Eulerian constrained scheme. Their Figs. 5a,b correspond to our Figs. 9g,h, their Figs. 4a,b correspond to our Figs. 9e,f, and their Figs. 3a,b correspond to our Figs. 9c,d. Taking the solutions of GC91 at 2.5-m resolution as reference for various values of diffusion coefficient (their Figs. 3c, 4c, and 5c for K = 0.25, 0.5, and 1.0

$m^2 s^{-1}$, respectively), the following conclusions are arrived at. With a very large diffusion coefficient ($K = 1$ $m^2 s^{-1}$), the SL solutions at 5-m resolution compare favorably with GC91 solution at 2.5-m resolution; the same is true comparing the 10-m SL with the 5-m GC91 result. When the mixing coefficient K is reduced to 0.5 $m^2 s^{-1}$, GC91 showed that very fine resolution (2.5 m) was required to prevent numerical noise from triggering false eddies at the cloud edge. In the SL integration, convergence of the solution is obtained at much coarser resolution than in GC91. The eddies developed by the SL at 10 and 5 m with $K = 0$ are of smaller dimension than those obtained by GC91 at 2.5 km with $K = 0.25$. In agreement with the conclusions derived from one-dimensional coupled advection–condensation experiments in the previous section, the dynamical integrations made with the unconstrained semi-Lagrangian scheme exhibit sharper details and a lower level of noise than even the higher-resolution integrations of GC91 obtained with a variant of the Eulerian scheme.

This experiment confirms the one-dimensional tests conclusions: the semi-Lagrangian scheme used on nondiscontinuous distributions does not appear to require, in practice, any constraint to prevent false evaporation. Due to the interpolative nature of the scheme, any numerical noise produced by this scheme is small enough that it is not harmful to the integrations.

4. Conclusions

The semi-Lagrangian transport scheme has been applied to a set of coupled field equations for internal energy, water vapor, and cloud water, the coupling being provided by phase changes of water substance. The one-dimensional version of these equations with a localized (discontinuous) cloud in a homogeneous environment subject to a prescribed constant vertical velocity was shown by Grabowski and Smolarkiewicz (1990) to be useful for assessing the ability (or lack thereof) of numerical schemes to maintain monotonicity in their solutions.

It has been shown in this paper that an SL scheme with unconstrained cubic interpolation does generate some ripples in fields that exhibit rapid variations. These ripples are, however, substantially weaker than in most Eulerian leapfrog schemes. The spurious ripples generated by the SL transport scheme may be amplified by condensations processed when abrupt concentration variations are present in the cloud or moisture fields. It has been shown that quasi-monotone constraints are insufficient to prevent the occurrence of spurious ripples in a problem with sources and sinks, as was first noted by Grabowski and Smolarkiewicz (1990) for a variant of the Eulerian scheme. Based on physical understanding of the false ripples problem, a fairly straightforward constraint has been devised that is effective in preventing their occurrences in this simplified test situation. Thus constrained, the SL scheme outperforms published results on this canonical problem. It is also shown that the SL scheme produces quite acceptable solutions, even without constraints, when the thermodynamic fields do not have discontinuities in their initial distributions.

Finally, a series of tests were made with a dynamical model, SISLAM, solving the fully elastic equations with a semi-implicit semi-Lagrangian scheme for a moist bubble convection experiment, trying to reproduce with (unconstrained) SL numerics the results of Grabowski and Clark (1991) obtained with a constrained variant of the Eulerian model. Our results show that the level of numerical noise of an SL model is less severe than in some Eulerian models and that similar results can be obtained with coarser resolution. It is noteworthy that SISLAM is approximately 20 times more efficient than most Eulerian models, owing to the combination of the possibility of using quite large time steps and the fact that a given level of accuracy can be obtained with coarser resolution (and hence fewer grid points).

These experiments lend confidence in the SL numerical scheme for modeling complex thermodynamic and dynamical processes. The SL scheme suffers from little numerical dispersion, and the simulated results appear to have less noise than many Eulerian, often more complicated and computationally costly, schemes.

Acknowledgments. The authors would like to pay tribute to the contribution of the late Professor André Robert (28 April 1929–18 November 1993), who directed the numerical component of the M.S. research of Pellerin (1992) from which this article evolved. André's enthusiasm for his research and his dedication to work will remain an example for all those who have worked with and for him. We would like to thank Dr. Wojciech Grabowski and an anonymous reviewer for their comments that contributed to improving our article. This research was sponsored by UQAM, Environment Canada, and Canadian National Science and Engineering Research Council Grants.

REFERENCES

Bergeron, G., R. Laprise, and D. Caya, 1994: The numerical formulation of the Mesoscale Compressible Community model. CCRM Report, 165 pp. [Available from Prof. R. Laprise, Department of Physics, UQAM, P.O. Box 8888, Stn "Downtown," Montréal, Québec, Canada H3C 3P8.]

Bermejo, R., and A. Staniforth, 1992: The conversion of semi-Lagrangian advection schemes to quasi-monotone schemes. *Mon. Wea. Rev.*, **120,** 2622–2632.

Boris, J. P., and D. L. Book, 1973: Flux-corrected transport I: SHASTA—A fluid transport algorithm that works. *J. Comput. Phys.*, **11,** 38–69.

——, and ——, 1976: Flux-corrected transport III: Minimal-error FCT algorithm. *J. Comput. Phys.*, **20,** 398–431.

Colella, P., and P. R. Woodward, 1984: The piecewise parabolic method (PPM) for gas-dynamical simulations. *J. Comput. Phys.*, **54,** 174–201.

Grabowski, W. W., and P. K. Smolarkiewicz, 1990: Monotone finite-difference approximations to the advection–condensation problem. *Mon. Wea. Rev.*, **118,** 2082–2097.

——, and T. L. Clark, 1991: Cloud–environment interface instability: Rising thermal calculations in two spatial dimensions. *J. Atmos. Sci.*, **48,** 527–546.

Mesinger, F., and A. Arakawa, 1976: Numerical methods used in atmospheric models. GARP Publ. Series 17, 64 pp.

Morse, B. J., 1973: An analytical study of mesh refinement applied to the wave equation. Part 1, NOAA Tech. Memo. ERL WMPO-5 (COM-73-11953-01), 1–14.

Ostiguy, L., and J. P. R. Laprise, 1990: On the positivity of mass in commonly used numerical transport schemes. *Atmos.–Ocean,* **28,** 147–161.

Pellerin, P., 1992: Validation d'un nouveau modèle numérique basé sur les équations d'Euler: Modèle UQAM de convection (Validation of a new numerical model based on the Euler equations: UQAM's convection model). M.S. thesis, University of Québec at Montréal, 79 pp. [Available from Prof. R. Laprise, Department of Physics, UQAM, P.O. Box 8888, Stn "Downtown," Montréal, Québec, Canada H3C 3P8.]

Rancic, M., 1992: Semi-Lagrangian piecewise biparabolic scheme for two-dimensional horizontal advection of a passive scalar. *Mon. Wea. Rev.*, **120,** 1394–1406.

Robert, A. J., 1981: A stable numerical integration scheme for the primitive meteorological equations. *Atmos.–Ocean.*, **19-1,** 35–46.

——, 1993: Bubble convection experiments with a semi-implicit formulation of the Euler equations. *J. Atmos. Sci.*, **50,** 1865–1873.

Rood, R. B., 1987: Numerical advection algorithms and their role in atmospheric transport and chemistry models. *Rev. Geophys.*, **25,** 71–100.

Smolarkiewicz, P. K., 1983: A simple positive definite advection scheme with small implicit diffusion. *Mon. Wea. Rev.*, **111,** 479–486.

——, and T. L. Clark, 1986: The multidimensional positive definite advection transport algorithm: Further development and applications. *J. Comput. Phys.*, **67,** 396–438.

——, and W. W. Grabowski, 1989: A multidimensional positive definite advection transport algorithm: Nonoscillatory option. *J. Comput. Phys.*, **86,** 355–375.

Tanguay, M., A. Robert, and R. Laprise, 1990: A semi-implicit semi-Lagrangian fully compressible regional forecast model. *Mon. Wea. Rev.*, **118,** 1970–1980.

Williamson, D. L., and P. J. Rasch, 1989: Two-dimensional semi-Lagrangian transport with shape preserving interpolation. *Mon. Wea. Rev.*, **117,** 102–129.